Nanoscale

COMMUNICATION

Tb^{3+}-doped LaF_3 nanocrystals for correlative cathodoluminescence electron microscopy imaging with nanometric resolution in focus ion beam-sectioned biological samples

Received 00th January 20xx,
Accepted 00th January 20xx

DOI: 10.1039/x0xx00000x

www.rsc.org/

K. Keevend,[a] M. Stiefel,[b] A. L. Neuer,[a] M. T. Matter,[a] A. Neels,[c] S. Bertazzo,[d,°] I. K. Herrmann[a,*]

Here, we report the use of rare earth element-doped nanocrystals as probes for correlative cathodoluminescence (CL) – electron microscopy (CCLEM) bioimaging. This first experimental demonstration shows potential for the simultaneous acquisition of luminescence and electron microscopy images with nanometric resolution in focus ion beam cut biological samples.

The invention of optical microscopes has enabled scientists to discover the existence of microorganisms and to study the structure and composition of cells and tissues.[1] The subsequent development of electron microscopes and procedures to analyse ultrastructural features revolutionized yet again our understanding of how living systems work.[2] Biological systems are vastly complex, and a better understanding of them heavily relies on the ability to see detailed relationships between structure and function at various levels of resolution and within a functionally correlated context.[3] However, the different imaging methods are based on specific physical principles, and have different resolutions leading to substantial technical challenges in reliable image acquisition and data correlation.

Correlative microscopy techniques can help bridging the mismatch in resolution between *e.g.*, light and electron microscopy, and provide a more comprehensive picture.[3-5] In order to acquire fluorescence images with resolutions higher than the Abbé diffraction limit (~λ/2), more refined techniques, such as stochastic optical reconstruction microscopy (STORM)[6] or stimulated emission depletion (STED) microscopy[7, 8] need to be employed.

Electron microscopy provides nanometric resolution. However, acquisition of high contrast electron microscopy images often requires sophisticated specimen preparation, and the use of suitable contrasting agents, such as osmium tetroxide and uranyl acetate, which typically quench fluorescence of organic fluorophores.[9] Additionally, exposure to high-energy electrons commonly used for the acquisition of electron micrographs leads to rapid degradation of organic fluorophores.[10] Therefore, it is often challenging to collect luminescence data and high contrast electron micrographs from the same sample.

Interestingly, a wide range of inorganic materials emit photons upon exposure to accelerated electrons, an effect known as cathodoluminescence (CL). This effect can be employed for optical imaging with spatial resolution in the nanometric range, as the resolution is primarily determined by the diameter of the focused electron beam, which scans the specimen.[11]

For high quality cathodoluminescence imaging, it is important to use stable fluorophores. Rare earth (RE) elements are known for their luminescent properties. RE ions have a number of advantages, including narrow spectral lines, sharp fluorescence emission and high photo-stability under laser and electron excitation.[12-14] In particular, lanthanum fluoride (LaF_3) is an outstanding host matrix for luminescent RE ions, by means of low phonon energy and high chemical stability. The LaF_3 matrix can be doped with different RE ions, such as terbium, dysprosium, europium, neodymium, *etc.*, due to their similar ionic radii.[15] Since the photoemission of rare earth element-doped inorganic nanocrystals is generally less affected by electron beam exposure compared to organic fluorophores, RE ion-doped nanoparticles are excellent imaging probes.[16]

Cathodoluminescence imaging using nanocrystal-based probes is a particularly appealing approach for correlative imaging as high-resolution CL data can be acquired simultaneously to electron micrographs. This in turn enables

[a]*Particles-Biology Interactions, Department of Materials Meet Life, Swiss Federal Laboratories for Materials Science and Technology (Empa), Lerchenfeldstrasse 5, 9014 St. Gallen, Switzerland. *inge.herrmann@empa.ch*
[b]*Reliability Science and Technology, Department of Materials Meet Life, Swiss Federal Laboratories for Materials Science and Technology (Empa), Uberlandstrasse 129, 8600 Dubendorf, Switzerland*
[c]*Center for X-ray Analytics, Department of Materials Meet Life, Swiss Federal Laboratories for Materials Science and Technology (Empa), Uberlandstrasse 129, 8600 Dubendorf, Switzerland*
[d]*Department of Medical Physics and Biomedical Engineering, University College London (UCL), Malet Place Engineering Building, London, WC1E 6BT, United Kingdom °s.bertazzo@ucl.ac.uk*

† Electronic Supplementary Information (ESI) available: Details of experiments, raw data and additional figures. See DOI: 10.1039/x0xx00000x

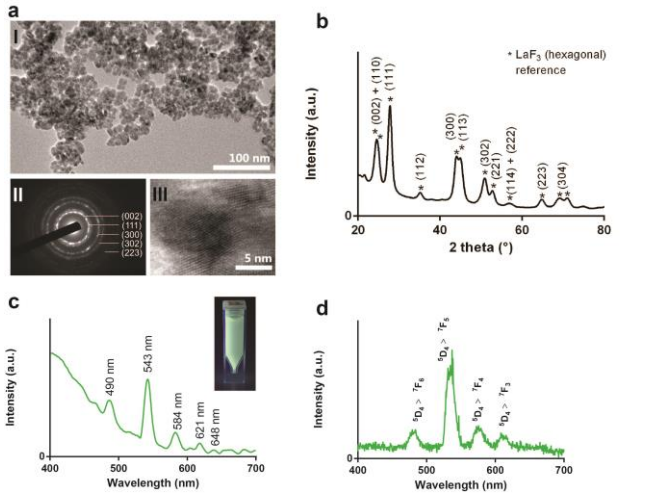

Figure 1: Transmission electron micrograph, electron diffraction patterns, high resolution transmission electron micrograph (a), and X-ray diffraction (XRD) patterns (b) of as-prepared Tb^{3+}-doped LaF_3 nanocrystals. The asterisked peaks correspond to reference data.[17] Photoluminescence spectrum of PEGylated Tb^{3+}-doped LaF_3 nanocrystals using excitation 346 nm (c). The inset is a photograph of Tb^{3+}-doped LaF_3 colloidal solution under 254 nm excitation. Corresponding cathodoluminescence spectrum of PEG-capped nanoparticles exposed to an electron acceleration beam of 5 kV (d).

optoelectronic characterisation of biological samples. A few studies on scanning electron microscope (SEM) and scanning transmission electron microscope (STEM) systems coupled with cathodoluminescence for studying biological systems using fluorescent nanoparticles have demonstrated promise.[16, 18, 19] RE-doped Y_2O_3 nanocrystals have been used for CL-STEM[16] and CL-SEM[20] (multicolour) cathodoluminescence bioimaging. While these studies have demonstrated the feasibility of cathodoluminescence bioimaging, the quality and resolution of images of biological samples in all these reports remain limited, mostly due to low contrast of the electron micrographs and the use of relatively large nanocrystals (primary particle diameter > 50 nm).

Here, we explore the use of Tb^{3+}-doped LaF_3 nanocrystals as probes for correlative cathodoluminescence electron microscopy imaging of biological specimen with nanometric resolution. We demonstrate that CL imaging of RE-doped LaF_3 nanocrystals can be used in combination with high resolution electron back-scattering imaging of osmium-contrasted biological samples, hence opening a new avenue to high resolution correlative imaging of nanometric objects and ultrastructural features of biological samples.

RE-doped LaF_3 crystals were synthesized by co-precipitation using either poly(ethylene glycol) (PEG) or poly(vinylpyrrolidone) (PVP) as capping agents. Transmission electron micrographs (TEM) of as-prepared nanocrystals show spherical primary particles with a narrow size distribution centered around 10 nm (Figure 1a (I)). Obtained electron diffraction patterns show highly crystalline nanoparticles (Figure 1a (II)). X-ray diffractometry (XRD) confirms the presence of a crystalline hexagonal LaF_3 phase (Figure 1b; see ESI, Figure S1).[21] The calculated crystallite size according to the Scherrer equation is 8 ± 2 nm, which is in line with TEM data. Fourier-transformed infrared spectroscopy (FTIR) analysis shows peaks characteristic for LaF_3 and organic capping agents and is in agreement with previous reports (see ESI, Figure S2).[15, 22] Thermogravimetric analysis (TGA) indicates a weight loss of 5% for PEGylated and 10% for PVP capped nanocrystals (see ESI, Figure S3), confirming primary functionalization of the particles. Characteristic photoemission peaks for Tb^{3+} were obtained from as-prepared nanocrystals using laser excitation with a wavelength of 346 nm (Figure 1c) and electron excitation using an acceleration voltage of 5 kV (Figure 1d). Obtained spectra coincide well with each other. The most intense emission was found around 540 nm in the visible range, corresponding to the $^5D_4 \rightarrow {}^7F_5$ transition.

In addition to luminescence, colloidal stability of LaF_3 nanocrystals in physiological media is particularly important with regard to the application as imaging probes. Nanoparticle tracking analysis (NTA) measurements show good stability of nanocrystals in cell culture media with average particle sizes (expressed as mode) of 135 nm and 163 nm for PEGylated and PVP-coated nanocrystals, respectively (Figures 2a and ESI, Figure S4). PEGylated nanocrystals also show remarkable colloidal stability over time in protein containing cell culture media (see ESI, Figure S5). The good colloidal stability is a consequence of the surface charge demonstrated by zeta potential measurements showing a mean zeta potential of -32.0 ± 3.8 mV for PEGylated nanocrystals and -10.0 ± 0.7 mV for PVP-coated LaF_3 nanocrystals.

In order to be suitable also for exposure scenarios involving live cells, luminescent nanocrystals should be harmless to cells. We therefore assessed cytotoxicity of RE-doped nanocrystals in a cytotoxicity assay. Lactate dehydrogenase (LDH) is an enzyme, which is released upon damage to the cellular membrane, and is a sensitive surrogate measure of cytotoxicity. Measurement of the LDH activity in cell culture supernatants after 24 hours of particle exposure to human lung cells (A549) shows LDH activities comparable to particle-free controls for all concentrations investigated (< 200 µg / 100'000 cells) (Figure 2b and ESI, Figure S6).

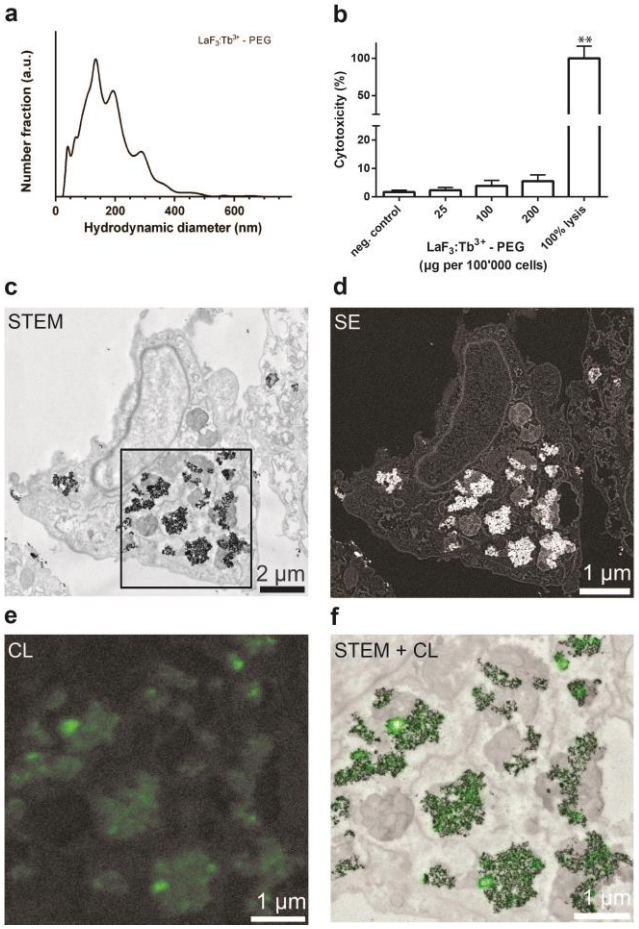

Figure 2: Hydrodynamic size measurements in physiological media (cell culture media) for PEGylated nanocrystals (a). Cytotoxicity measurements showing the release of lactate dehydrogenase from human A549 cells in response to particle exposure (0-200 µg per 100'000 cells) for 24 hours (expressed relative to 100% lysis) (b). Scanning transmission electron micrographs (STEM) (c) and corresponding secondary electron image (d) showing intracellular particle agglomerates. Cathodoluminescence image of the corresponding area with a pixel size of 20 nm (e) and an overlay image of a brightfield-STEM image and corresponding CL-image, showing co-localization of the particles (f).

Cellular uptake of LaF_3 nanocrystals was confirmed by scanning transmission electron micrographs (STEM) of cells exposed to particles for 24 hours. STEM images of 100 nm sections show particle aggregates localized in vesicular structures as well as nanoparticles sticking to the outer cell membrane (Figure 2c and ESI, Figure S7). Nanoparticles are taken up by cells by an endocytosis mechanism and are predominately localized inside of endosomes. The intracellular distribution of the particles can be seen in Figure 2c. Based on the hydrodynamic size of the particles, they are most likely engulfed by a micropinocytosis mechanism.[23] Simultaneously to STEM, we acquired secondary electron (Figure 2d) and cathodoluminescence signal (Figure 2e) from the same region, obtaining information about elemental contrast and optical properties of the sample. CL-images of 100 nm sections of A549 cells were recorded and show nanoscale resolution (< 50 nm) with pixel sizes of 20 nm and 2 nm, respectively (see Figure 2e and ESI, Figure S8. For unprocessed cathodoluminescence images, see ESI, Figure S9). Low voltages have been used for CL imaging for optimal spatial resolution and to minimize bleaching. Recorded cathodoluminescence images coincide well with the STEM images from the same region (Figure 2f). The CL-resolution is significantly higher compared to the Abbé diffraction limit typically encountered in optical imaging (> 200 nm). Interestingly, STEM images also show some particles located outside of endosomes, which is most likely due to a mechanical artefact caused by the sectioning in the ultra- microtome (see ESI, Figures S10, the arrow indicates particles outside of vesicular bodies). It is unlikely that particles of this size are present outside of vesicular compartments.[24] This hypothesis is further supported by the fact that extravesicular particles are only found in the movement direction of the cutting blade relative to the vesicle.

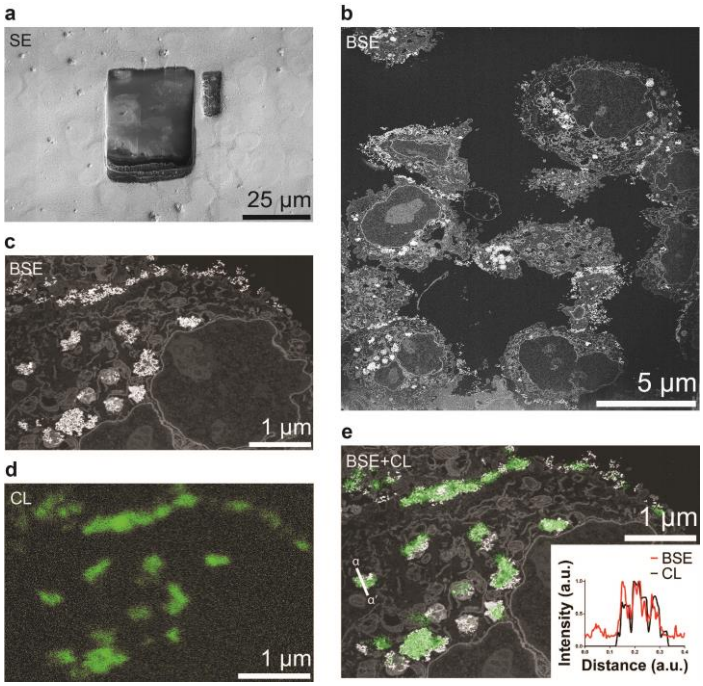

Figure 3: Trench cut with a focused ion beam (FIB, gallium ion beam). Individual cells on the resin block face and the cross-section can easily be recognized in the secondary electron image (a). Electron backscattering image of the FIB cross-section (b). Electron back-scattering image of a single cell (c) and corresponding cathodoluminescence image (d) with a pixel size of 50 nm. Overlay image showing co-localization of the particles in the BSE and the CL image. The inset presents the profile of normalized cathodoluminescence and back-scattering signal, showing co-localization of the signals (e).

Finally, we investigated the prospect of using focused ion beam (FIB) sectioning and subsequent imaging of the cross-section of resin-embedded biological samples using secondary electron (SE), electron backscattering (BSE) and CL signals. FIB-SEM imaging is a powerful high-resolution imaging technique, which enables slice-and-view imaging with nanometric resolution in x-y-z.[25] The beam current of the ion beam is tuneable over a wide range, allowing milling of large areas and enabling greater imaging volumes. Also, the geometry of the instrument allows changing imaging angles, which in the end provides additional flexibility in regard to data acquisition. Here, a focused gallium ion beam was used to cut a trench and expose a cross-section of 40 µm x 50 µm (Figure 3a, b). Cells and their ultrastructural features, including mitochondria, vesicular and nuclear membranes, and the nucleolus could easily be identified in the backscattering electron channel (Figure 3b, c). Simultaneously to the electron microscopy images acquisition, CL intensity maps of the FIB cross-section were acquired. The use of a filter (525-575 nm) allowed detection of Tb^{3+}-specific emission associated with the nanocrystals, which is displayed as a map in Figure 3d (for unprocessed cathodoluminescence images, see ESI, Figure S9). The green emission again generally coincided well with particle localization seen in the backscattering image, however, some slight misalignment due to charging is observed. Unlike classical fluorescence, which is quenched, the CL signal intensity was not negatively affected neither by the presence of osmium tetroxide nor epoxy embedding. This in turn enables correlative acquisition of high contrast electron micrographs showing the ultrastructure of the cells and high resolution CL images in SEM mode (Figure 3e). However, prolonged exposure of the Tb^{3+}-doped polymer-capped LaF_3 nanoparticles to electron beam irradiation showed that the stability of the nanocrystals is limited (see ESI, Figure S11). The decrease in CL-intensity over time can most likely be attributed to knock-on damage to the nanoparticles, which has previously been described by Sun *et al*. for $NaREF_4$ nanoparticles under high voltage (200 kV) electron beam irradiation.[26] Hence, nanocrystal properties need to be further optimized to address stability issues, especially when using low scanning speed for CL image acquisition.

This first experimental demonstration of correlative cathodoluminescence-backscattering electron microscopy on FIB-sectioned biological samples illustrates the potential of the approach for the acquisition of high-quality luminescence and electron microscopy images with nanometric resolution. We demonstrate optoelectronic characterization of resin-embedded biological samples contrasted with osmium tetroxide, harvesting the different sample specific emissions of electrons (SE, BSE) and photons (CL) upon electron beam exposure. RE-doped LaF_3 nanocrystals show promise for correlative microscopy and could potentially be used as molecular labels owing to their small size, high colloidal stability and bright emission upon both laser and electron beam exposure. In addition to Tb^{3+}, other RE-ions can be employed in a similar setting. It is important to note that while the use of high energy excitation wavelengths required for the excitation of Tb^{3+} is generally unfavourable in the case of live cell imaging and in vivo applications, the CCLEM samples are embedded in epoxy resins and exposed up to 80 kV during the acquisition of electron micrographs. Hence, the radiation damage to the biological sample caused by cathodoluminescence imaging is negligible. However, oxide-based matrices should preferably be used for 3D CCLEM imaging, where high electron beam exposure times are expected.

The proposed FIB-based method may in future enable simultaneous molecular labelling and structural imaging based on nanocrystals with nanometric resolution in the three-dimensional space, using a single instrument.[27] Correlative cathodoluminescence - electron microscopy bioimaging opens new avenues for the optoelectronic investigation of structure-function relationships at the nanoscale. It allows distinction of nanoparticle-based labels from naturally occuring granules (such as glycogen granules[28]), which often is challenging in traditional electron microscopy.[29, 30] Additionally, CCLEM can be used as a multicolour imaging platform, where different structures can be labelled with nanocrystals hosting different RE-ions, hence featuring different colours.

Acknowledgements

We thank Liliane Diener for ultramicrotome sectioning of the embedded samples, Urs Bünter for taking photographs of the luminescent nanoparticles, and Yvonne Elbs-Glatz and Dr Nils Bohmer for their assistance in cell culture.

Nanoscale

COMMUNICATION

References

1. I. Ghiran, in *Light Microscopy*, eds. H. Chiarini-Garcia and R. C. N. Melo, Humana Press, 2011, vol. 689, ch. 7, pp. 93-136.
2. T. F. Anderson, *Transactions of the New York Academy of Sciences*, 1951, **13**, 130-134.
3. B. N. G. Giepmans, S. R. Adams, M. H. Ellisman and R. Y. Tsien, *Science*, 2006, **312**, 217-224.
4. B. G. Kopek, G. Shtengel, C. S. Xu, D. A. Clayton and H. F. Hess, *Proceedings of the National Academy of Sciences*, 2012, **109**, 6136-6141.
5. M. R. G. Russell, T. R. Lerner, J. J. Burden, D. O. Nkwe, A. Pelchen-Matthews, M.-C. Domart, J. Durgan, A. Weston, M. L. Jones, C. J. Peddie, R. Carzaniga, O. Florey, M. Marsh, M. G. Gutierrez and L. M. Collinson, *Journal of Cell Science*, 2016, DOI: 10.1242/jcs.188433.
6. M. J. Rust, M. Bates and X. Zhuang, *Nature Methods*, 2006, **3**, 793-796.
7. K. I. Willig, S. O. Rizzoli, V. Westphal, R. Jahn and S. W. Hell, *Nature*, 2006, **440**, 935-939.
8. S. Watanabe, A. Punge, G. Hollopeter, K. I. Willig, R. J. Hobson, M. W. Davis, S. W. Hell and E. M. Jorgensen, *Nature Methods*, 2011, **8**, 80-84.
9. M. S. Lucas, *Correlative Light Electron Microscopy*, Elsevier, 2012.
10. K. Nagayama, T. Onuma, R. Ueno, K. Tamehiro and H. Minoda, *The Journal of Physical Chemistry B*, 2016, **120**, 1169-1174.
11. B. G. Yacobi and D. B. Holt, *Cathodoluminescence Microscopy of Inorganic Solids*, Springer, 1990.
12. S. Fukushima, T. Furukawa, H. Niioka, M. Ichimiya, J. Miyake, M. Ashida, T. Araki and M. Hashimoto, *Micron*, 2014, **67**, 90-95.
13. S. Fukushima, T. Furukawa, H. Niioka, M. Ichimiya, T. Sannomiya, N. Tanaka, D. Onoshima, H. Yukawa, Y. Baba, M. Ashida, J. Miyake, T. Araki and M. Hashimoto, *Scientific Reports*, 2016, **6**, 25950.
14. S. Gai, C. Li, P. Yang and J. Lin, *Chemical Reviews*, 2014, **114**, 2343-2389.
15. F. Li, Li, C., Liu, X., Bai, T., Wenjun, D., Zhang, X., Shi, Z., Feng, S., *Dalton Transactions*, 2013, **42**, 2015-2022.
16. T. Furukawa, S. Fukushima, H. Niioka, N. Yamamoto, J. Miyake, T. Araki and M. Hashimoto, *Journal of Biomedical Optics*, 2015, **20**, 056007-056007.
17. d. R. C., T. G. and Z. C., *Comptes Rendus Hebdomadaires des Seances de l'Academie des Sciences, Serie C, Sciences Chimiques* 1966, **263**, 64-66.
18. S. Nagarajan, C. Pioche-Durieu, L. H. G. Tizei, C.-Y. Fang, J.-R. Bertrand, E. Le Cam, H.-C. Chang, F. Treussart and M. Kociak, *Nanoscale*, 2016, **8**, 11588-11594.
19. D. R. Glenn, H. Zhang, N. Kasthuri, R. Schalek, P. K. Lo, A. S. Trifonov, H. Park, J. W. Lichtman and R. L. Walsworth, *Scientific Reports*, 2012, **2**, 865.
20. N. Hirohiko, F. Taichi, I. Masayoshi, A. Masaaki, A. Tsutomu and H. Mamoru, *Applied Physics Express*, 2011, **4**, 112402.
21. S. Gražulis, D. Chateigner, R. T. Downs, A. F. T. Yokochi, M. Quirós, L. Lutterotti, E. Manakova, J. Butkus, P. Moeck and A. Le Bail, *Journal of Applied Crystallography*, 2009, **42**, 726-729.
22. K. Shameli, M. Bin Ahmad, S. D. Jazayeri, S. Sedaghat, P. Shabanzadeh, H. Jahangirian, M. Mahdavi and Y. Abdollahi, *International Journal of Molecular Sciences*, 2012, **13**, 6639.
23. L. Kou, J. Sun, Y. Zhai and Z. He, *Asian Journal of Pharmaceutical Sciences*, 2013, **8**, 1-10.
24. S. Zhang, H. Gao and G. Bao, *ACS Nano*, 2015, **9**, 8655-8671.
25. K. Narayan and S. Subramaniam, *Nature Methods*, 2015, **12**, 1021-1031.
26. X. Sun, B. Wang, I. Kempson, C. Liu, Y. Hou and M. Gao, *Small*, 2014, **10**, 4711-4717.
27. K. Narayan, C. M. Danielson, K. Lagarec, B. C. Lowekamp, P. Coffman, A. Laquerre, M. W. Phaneuf, T. J. Hope and S. Subramaniam, *Journal of Structural Biology*, 2014, **185**, 278-284.
28. I. K. Herrmann, S. Bertazzo, D. J. P. O'Callaghan, A. A. Schlegel, C. Kallepitis, D. B. Antcliffe, A. C. Gordon and M. M. Stevens, *Nanoscale*, 2015, **7**, 13511-13520.
29. C. Brandenberger, M. J. Clift, D. Vanhecke, C. Mühlfeld, V. Stone, P. Gehr and B. Rothen-Rutishauser, *Particle and Fibre Toxicology*, 2010, **7**, 15.
30. C. Mühlfeld, B. Rothen-Rutishauser, D. Vanhecke, F. Blank, P. Gehr and M. Ochs, *Particle and Fibre Toxicology*, 2007, **4**, 11.